Journal of Molecular Structure 938 (2009) 245–253

Contents lists available at ScienceDirect

Journal of Molecular Structure

journal homepage: www.elsevier.com/locate/molstruc

Synthesis and quantum chemical study of PDI derivatives with phenylalkynyl groups at the bay position

Delou Wang, Yan shi, Chuntao Zhao, Baolong Liang, Xiyou Li *

Key Lab for Colloid and Interface Chemistry of Education Ministry, Department of Chemistry, Shandong University, China 250100, China

ARTICLE INFO

Article history:
Received 15 July 2009
Received in revised form 17 September 2009
Accepted 19 September 2009
Available online 26 September 2009

Keywords:
PDI
Phenylalkynyl
TD-DFT
Absorption spectra
Fluorescence spectra

ABSTRACT

Six new perylenetetracarboxylic diimide (PDI) compounds were prepared by introducing alkynyl or alkynylphenyl groups with different length to the bay position of PDI ring. The UV–vis absorption and emission spectra of these new compounds were recorded. The red-shift on the maximum absorption and emission peaks revealed the efficient participation of the side conjugation chain to the whole conjugation system. The molecular structure, the frontier molecular orbital and the energy gaps between the highest occupied orbital (HOMO) and the lowest un-occupied orbital (LUMO) were calculated with DFT method. The results show good consistent with the experimental results. The absorption and emission spectra of these six compounds were also simulated with TD-B3lyp/6-31g(d) and TD-PBE1PBE/6-31g(d) methods. The simulated results for the compounds with short side conjugation chain show better response to the experimental results. However, the quantum calculation on the compounds with long conjugated side chain do not give satisfied results because of the significant electron transfer characteristics in the excited states.

1. Introduction

Perylene-3,4,9,10-tetracarboxylic diimide (PDI) derivatives have attracted increasing attention in the past decade due to their outstanding photochemical and thermal stabilities, ease of synthetic modification, and desirable optical and redox characteristics. Great application potentials have been revealed in the fields of organic filed effect transistors (OFETs) [1,2], organic light emitting diodes (OLED) [3,4] electrostatic photographic copying devices [5], solar cells [6,7], molecular electronics [8,9], as well as artificial light harvesting system [10,11]. In order to meet the needs of different applications, PDIs with different structures and properties have been prepared [12].

The structure modification of PDIs has been achieved by introducing side groups either to the imide nitrogen atoms or at the bay positions, i.e. 1, 6, 7, 12 positions. Incorporation of substituents to the imide nitrogen atoms can significantly improve the solubility of corresponding PDI derivatives in conventional organic solvents and affect the packing model of PDI molecules in solid films [13–15]. But, it can not significantly affect the electronic structure and photophysical properties of PDI compounds because of the orbital nodes on the imide nitrogen atoms in both the HOMO and LUMO of PDI, which limit the electronic interactions between PDI and corresponding substituents [16]. In contrast, substituents at the bay positions of PDI were demonstrated to significantly affect the electronic properties, including electronic absorption spectra, fluorescence spectra, and redox potentials [17–19]. The substituents that have previously been incorporated onto the bay positions of PDIs are limited to phenoxy groups [20,21], aryls [22], cyclic secondary amines [23,24], cyano groups [25], halogens [26], and alkoxy and/or alkythio groups [27]. Very recently, alkynyl groups have been successfully introduced to the bay positions of PDI by Sonogashira reactions [28]. The absorption and emission spectra have been varied by the alkynyl groups significantly.

In the present work, we describe the synthesis and photophysical properties of a series of novel PDIs with phenylalkynyl groups of different length at the bay position of the PDI ring, **1**–**6** in Scheme 1. As opposed to the previous reported PDI compounds, which contains only one alkynyl group, the PDIs of this research have several alkynyl groups linked by phenyl rings and formed a long conjugated chain. This long linear aromatic substituent is expected in one hand to change the absorption and emission spectra significantly and on the other hand to provide a reaction point for connection of other groups.

2. Results and discussion

2.1. Molecular design and synthesis

The introduction of only one alkynyl group at the bay position of PDI has been achieved by Sonogashira reaction [28] in literature.

* Corresponding author.
E-mail address: xiyouli@sdu.edu.cn (X. Li).

0022-2860/$ - see front matter © 2009 Elsevier B.V. All rights reserved.
doi:10.1016/j.molstruc.2009.09.035

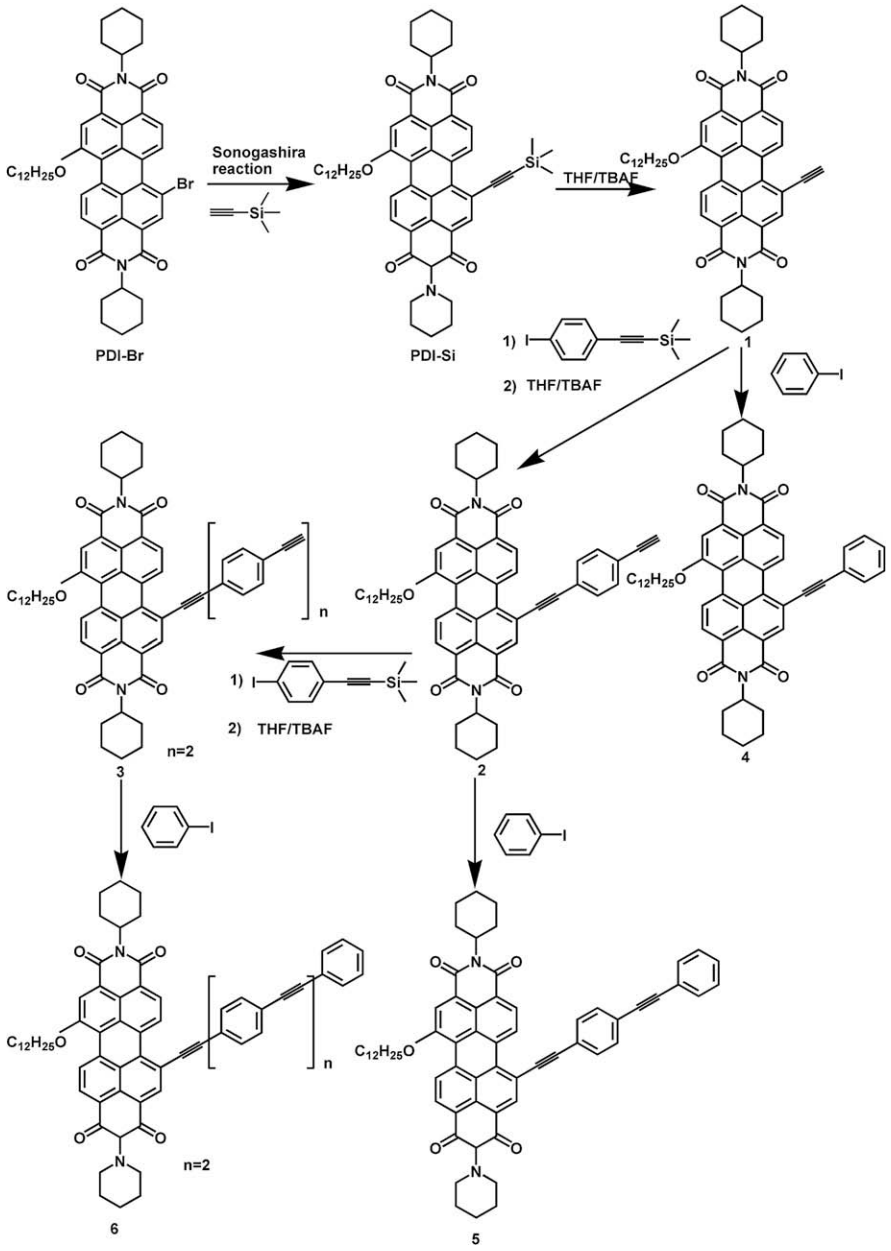

Scheme 1. Synthesis of PDI derivatives containing terminal alkynes and terminal benzene.

With this method, we successfully prepared PDI-Si in reasonable yields. After been hydrolyzed by tetra-*tert*-butyl ammonium fluoride, PDI-Si changed into **1**. However, when we try to prolong the aromatic arm by reacting **1** with 1-bromobenzene or *p*-bromophenyl-alkynyl, the reaction failed to give the title compound because of the reactivity dropping caused by the electron withdrawing nature of PDI ring. However, the iodide derivatives can reacts with **1** readily, therefore 1-iodid-4-(2-trimethylsilyl)alkynyl-benzene was prepared as an important intermediate to **2** and **3**, Scheme 2. The terminal alkynyl groups of **1**–**3** are caped with phenyl group by Sonogashira reactions to produce **4**, **5** and **6**, respectively, Scheme 1. In addition, **2** can also be synthesized by the reaction of PDI-Br with 1,4-dialkynylbezene with a yield of 6.3%.

2.2. Absorption spectra

The absorption spectra of these series of compounds are shown in Fig. 1 and the data are summarized in Table 1. Two absorption bands were observed in the visible region, which can be assigned to the absorption of PDI ring. The absorption bands in the region of 300–400 nm are due to the absorption of alkynylphenyl chain,

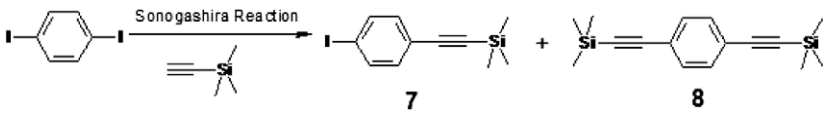

Scheme 2. Synthesis of intermediate **7**.

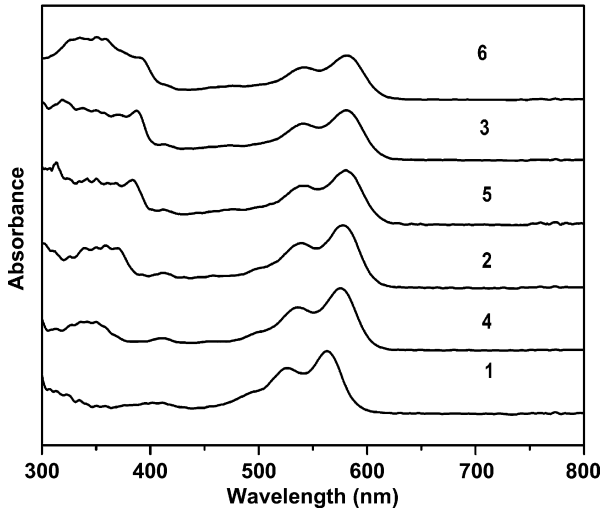

Fig. 1. UV–vis absorption spectra of compounds **1**–**6** in chloroform.

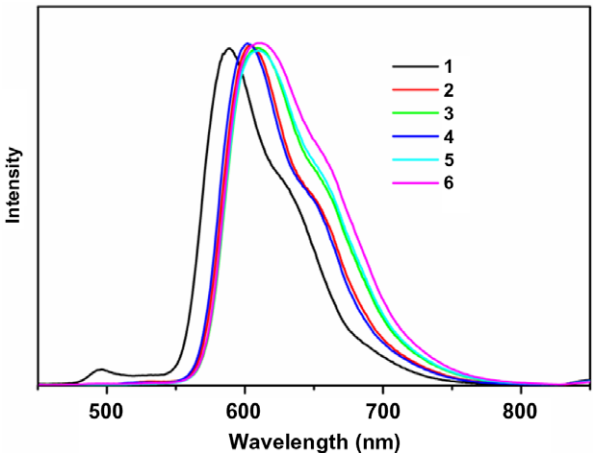

Fig. 2. Normalized fluorescence spectra of compounds **1**–**6** in chloroform with excitation at 410 nm.

Table 1
Photophysical properties of compounds **1**–**6**.

Compounds	λ_{abs} (nm)	ε (mol^{-1} L cm^{-1})	λ_{em} (nm)	Φ_f (%)	τ (ns)
1	563	5.62×10^4	589	97.2	5.80
2	578	5.00×10^4	604	91.0	6.75
3	581	5.05×10^4	615	67.6	7.60
4	575	5.02×10^4	602	81.0	6.82
5	580	4.96×10^4	610	72.3	7.41
6	581	4.90×10^4	620	76.0	7.44

which increased significantly in intensity and redshifted on the wavelength along with the increase on the length of the substituent. The maximum absorption band in the visible region of the PDIs shifted to red relative to their bromide precursor due to the extension of the conjugation.

The maximum absorption peak of **1** appears at 589 nm, which red shifted for about 16 nm relative to the PDI with only one dodecyloxyl group. Further addition of one phenyl group red shifted the maximum absorption peak to 581 nm in **3**. With the increasing on the distance of the alkynyl or phenyl group from the PDI core, the red-shift effects of the alkynyl or phenyl groups on the maximum absorption peak decreased remarkably. For example, the first phenyl group in **4** redshifted the maximum absorption peak for about 18 nm, the second phenyl group in **5** redshifted the maximum absorption peak for only 2 nm while the third phenyl group in **6** do not redshift the maximum absorption peak at all. Similar effects were found for the alkynyl groups too.

2.3. Fluorescence spectra

Fig. 2 shows the fluorescence spectra of these new PDI compounds in chloroform. As expected, the emission peaks significantly redshifted because of the introduction of alkynyl and phenyl groups. Along with the increasing on the length of the conjugated side chain, the magnitude of the redshifts on the emission peak varied follow the same order as that observed for the absorption maximum. Both the fluorescence quantum yields and lifetimes are measured for these series compounds. The results are also summarized in Table 1. As can be seen from the data, the introduction of the conjugated chain at the bay position of PDI induced significant decrease on the fluorescence quantum yields and remarkably prolonged fluorescence lifetimes. The smallest fluorescence quantum yield was presented by **3**, which has the second longest conjugated side chain, not by the PDI (**6**) with the longest conjugated side chain among these series of compounds.

2.4. Theoretical simulation on the molecular structure and electronic spectra

In order to understand the experimental results in deep, the ground state molecular structure, the frontier molecular orbital distributions, the HOMO/LUMO energy gaps as well as the absorption and emission spectra of these six PDI compounds are calculated. In order to save the calculating time, the molecular structures were simplified by replacing the dodecyloxy group with methoxyl group and cyclohexyl groups with methyl groups.

2.4.1. Minimized molecular structure

Using b3lyp/6-31g(d) method, the minimized structure of compounds **1**–**6** were optimized, Fig. 3. The calculated geometric parameters, including bond length and torsion angle between two naphthalene rings are listed in Table 2. In order to examine the accuracy of this method, a PDI compound without substituents at the bay positions, compound **9**, with known crystal structure is calculated [29]. Table 3 compares the calculated results with the crystal data. The calculated values are basically in line with the experimental values, indicating that the calculating method used is reliable for the calculation of this kind of compounds.

For the unsubstituent compound **9**, the torsion angle α between two naphthalene nucleuses basically is 0°. But when alkynyl and alkoxyl groups were introduced at the bay positions, the torsion angle between two naphthalene nucleuses increased to about 14–17.5° because of the steric hindrance. The conjugated chain growth does not influence the torsion angle significantly, probably because the steric hindrance is predominately determined by the first atom of the side group which directly connected to the PDI ring as reported previously [30].

2.4.2. Calculated frontier molecular orbital

The energy levels of the frontier molecular orbital HOMO-5 to LUMO+5 of **1**–**6** are listed in Fig. 4. Along with the increase on the length of the side conjugation substituent, the HOMO/LUMO energy gap decrease gradually as shown in Fig. 4. The decrease on the energy gap of HOMO/LUMO is caused mainly by the increase on the energy level of HOMOs. The energy gap between HOMO and LUMO decrease following the order of **1** > **4** > **2** > **5** > **3** > **6**, which is in accordance with the redshift on the maximum absorption peaks in the experimental recorded absorption spectra.

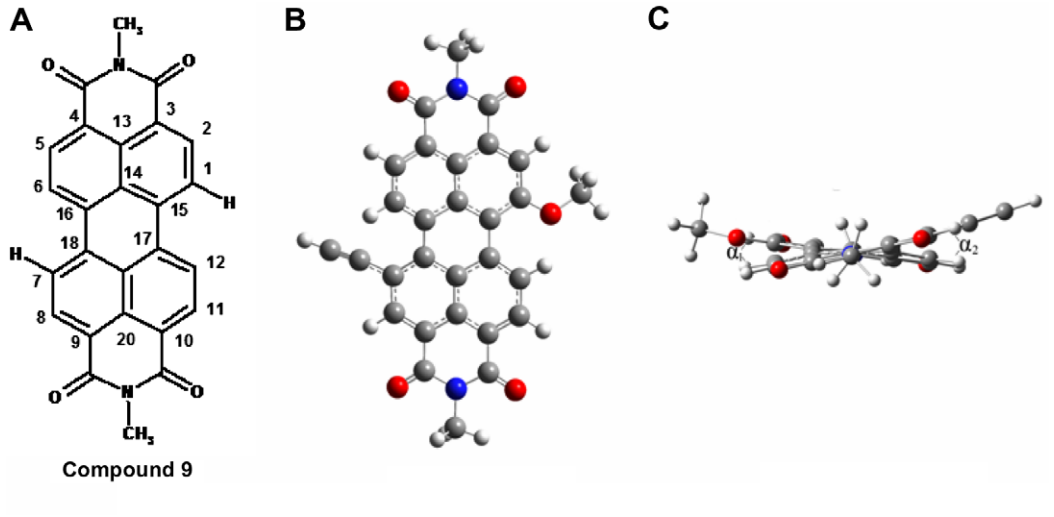

Fig. 3. The molecular structure of compound **9** (A) and the minimized molecular structure of **2** (B and C).

Table 2
The geometric construction parameters of PDI derivatives.

Parameter	1	2	3	4	5	6
C_1–C_2	1.406	1.406	1.406	1.405	1.405	1.406
C_2–C_3	1.379	1.379	1.379	1.379	1.379	1.379
C_3–C_{13}	1.411	1.411	1.411	1.411	1.411	1.411
C_{18}–C_7	1.419	1.421	1.422	1.421	1.422	1.422
C_7–C_8	1.416	1.418	1.418	1.418	1.418	1.418
C_8–C_9	1.376	1.374	1.374	1.374	1.374	1.374
C_9–C_{20}	1.415	1.417	1.417	1.417	1.417	1.417
C_{20}–C_{19}	1.430	1.430	1.430	1.430	1.430	1.430
C_{20}–C_{10}	1.414	1.413	1.413	1.413	1.413	1.413
C_{10}–C_{11}	1.383	1.384	1.384	1.384	1.384	1.384
C_{11}–C_{12}	1.397	1.397	1.397	1.397	1.397	1.397
C_{12}–C_{17}	1.402	1.402	1.402	1.402	1.402	1.402
C_{17}–C_{15}	1.469	1.469	1.469	1.469	1.469	1.469
C_{19}–C_{17}	1.439	1.438	1.439	1.438	1.438	1.439
C_{19}–C_{18}	1.433	1.4326	1.433	1.433	1.432	1.433
C_1–R_1	1.359	1.359	1.359	1.360	1.360	1.359
C_7–R_2	1.430	1.422	1.421	1.422	1.421	1.421
α_1	14.08	14.31	14.11	13.98	14.11	14.10
α_2	16.64	17.38	17.17	16.95	17.08	17.15

Table 3
The theoretical calculated bond length and the crystal data of compound **9.**

Bonds[a]	Calculated	Experimental[b]
C_1–C_2	1.399	1.396
C_2–C_3	1.384	1.365
C_3–C_{13}	1.416	1.422
C_{13}–C_{14}	1.429	1.409
C_{13}–C_4	1.416	1.422
C_4–C_5	1.384	1.365
C_5–C_6	1.399	1.396
C_6–C_{16}	1.396	1.383
C_{16}–C_{18}	1.471	1.457
C_{14}–C_{15}	1.431	1.423
C_{14}–C_{16}	1.431	1.423
α	−0.008	−1.188

[a] See Fig. 3 for atomic labels.
[b] Experimental data are taken from Ref. [29].

The calculated HOMO and LUMO orbital maps of these series of compounds revealed that the conjugation has fully extended to the alkynylphenyl chain. Fig. 5 shows the LUMO and HOMO orbital maps of **3** and **6** as representatives, while the contribution of the conjugated substituent for **1** to **6** are summarized in Table 4. It

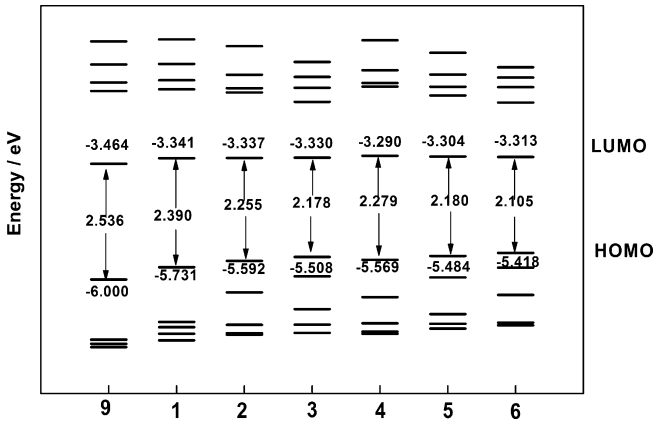

Fig. 4. The molecular orbital energy and HOMO/LUMO energy gaps of **1**–**6**.

can be found that even in compound **6**, which has the longest side conjugation chain, the HOMO orbital can extend to the end of the side chain.

The conjugated substituents have a significantly larger proportion in HOMO than that in LUMO, Table 4. The difference between the contribution of conjugation substituent in HOMO and LUMO increases along with the increasing in length of the substituent. Because of the larger difference on the contribution of substituent to the HOMO and LUMO, the transition from HOMO to LUMO under photoexcitation will induce electron cloudy flow from substituent to PDI ring and thus endow the excited states of these series of compounds with partial electron transfer characteristics. The electron transfer characteristic of the excited states will be more significant along with the increase on the length of the conjugated substituent because of the increasing distance between the positive and negative charge center. This large electron transfer characteristic will induce significant drop on the fluorescence quantum yields, which consists with the experimental recorded fluorescence quantum yields of these compounds.

2.5. Simulated UV–vis absorption spectra

TD-DFT can be effective for the excited states of the medium-sized molecules, so it become a very popular excited states simulation method. However, due to the general electron

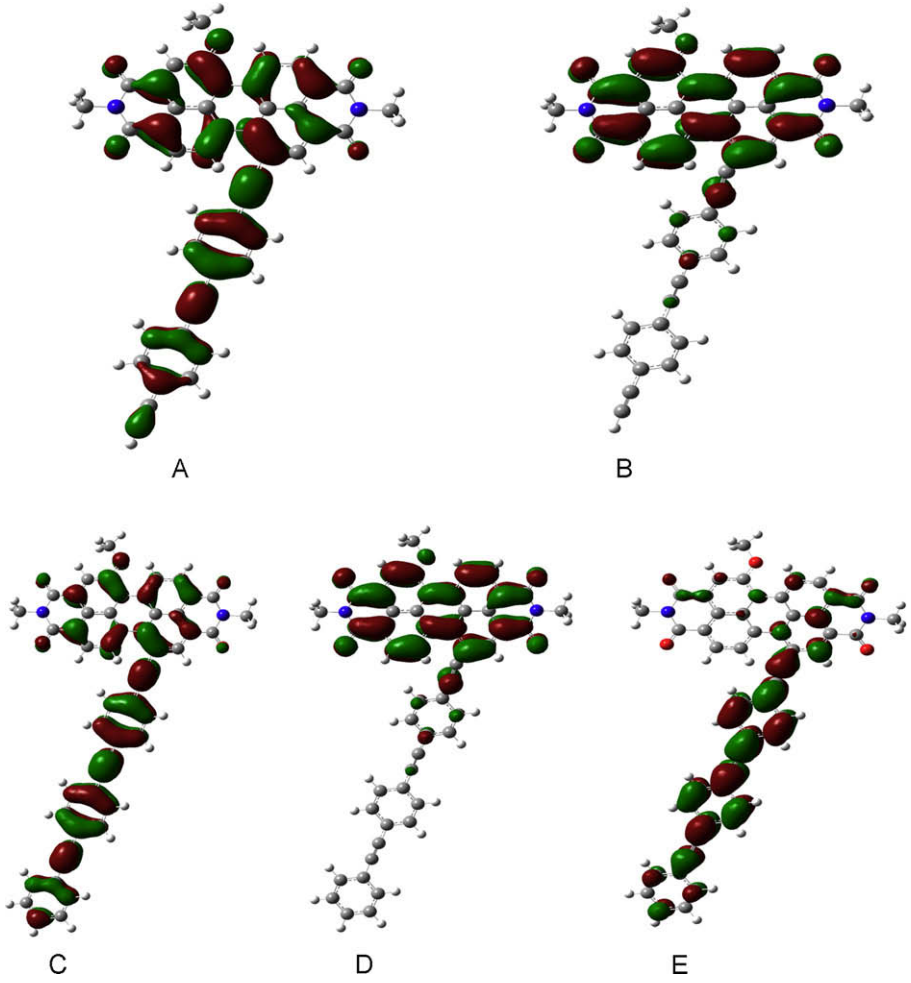

Fig. 5. Calculated molecular orbitals of **3** and **6**: (A) HOMO of **3**; (B) LUMO of **3.**

Table 4
The contribution of the substitutent to the HOMO and LUMO.

	1 (%)	**2** (%)	**3** (%)	**4** (%)	**5** (%)	**6** (%)
HOMO	4.73	20.43	39.61	16.14	37.29	59.40
LUMO	2.93	6.50	7.18	5.63	6.75	7.16

exchange–correlation functional can not well descript the role of long-range electron correlation in larger conjugate system and the excited states with charge transfer characteristic, TD-DFT calculation always leads to results with larger difference from the experimental results [31,32]. But the exact expression of the HF (Hartree–Fock) exchange energy can better descript the long-range electronic interactions, so when a larger charge transfer occurs in the excited states, we can use hybrid functionals that contain a higher proportion of HF to predict the experimental data [33,34]. We choose b3lyp and PBE1PBE to simulate the absorption spectra of **1** to **6**, because both of them are the hybrid functionals contain higher proportion of HF (b31yp 20% and PBE1PBE 25%).

With TD-B3lyp/6-31g(d) and TD-PBE1PBE/6-31g(d) methods, the absorption spectra of **1**–**6** were simulated. The maximum absorption peaks calculated are summarized in Table 5. The calculated results of TD-B3lyp/6-31g(d) for the compounds with short side conjugation chain are relatively more close to the experimental results. But for the compounds with long side conjugation chain, the calculated results of TD-PBE1PBE/6-31g(d) method seem more accurate relative to the experimental results. The simulated

Table 5
Use TD-b3lyp/6-31g(d) and TD-PBE1PBE/6-31g(d) calculated maximum absorption wavelength and experimental value of PDI compounds.

Compound	B3lyp			PBE1PBE			λ(exp)/nm
	λ/nm	*E*/eV	*f*	λ/nm	*E*/eV	*f*	
1	546	2.27	0.5571	531	2.34	0.5828	563
2	593	2.09	0.4646	572	2.17	0.4996	578
3	627	1.98	0.4692	596	2.08	0.5233	581
4	583	2.13	0.4698	564	2.20	0.5001	575
5	625	1.98	0.4457	596	2.08	0.4964	580
6	655	1.89	0.4494	613	2.02	0.5283	581

absorption spectra of **1** and **6** are shown in Fig. 6 as representatives. It can be found that the simulated absorption spectra of compound **1** based on TD-B3lyp/6-31g(d) show good similarity with the experimental recorded spectra. The maximum absorption at 546 nm due to the transition from HOMO to LUMO corresponding well with the experimental recorded absorption peaks at 527 and 560 nm. The small peak at about 300 nm can be assigned to the transition from HOMO-11 to LUMO, which can be ascribed to the absorption of side conjugation chain. The simulated results based on both TD-B3lyp/6-31g(d) and TD-PBE1PBE/6-31g(d) methods for other compounds were found diverse from the experimental results seriously especially for that with longer conjugation side chain. The simulated results for compound **6** based on PBE1PBE/6-31g(d) method as shown in Fig. 6 presents three main peaks, two of them at 614 and 518 nm are assigned to the transition of

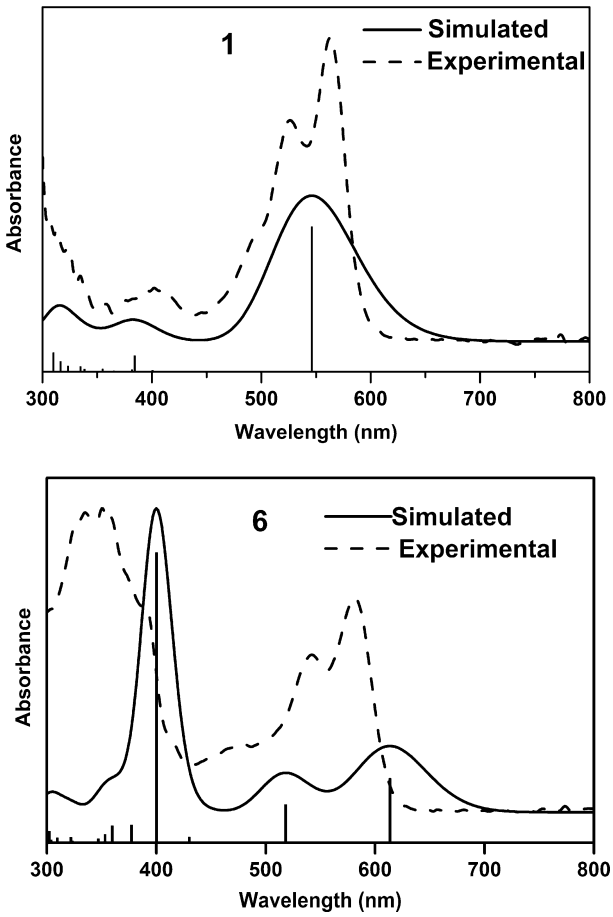

Fig. 6. The experimental and simulated absorption spectra of **1** and **6** (**1**, b3lyp. **6**, PBE1PBE).

HOMO to LUMO and HOMO-1 to LUMO respectively, which departure from the experimentally recorded two peaks at 581 and 541 nm significantly. The largest absorption peak in the simulated absorption spectra at 400 nm is assigned to the transition from HOMO to LUMO+1. The LUMO+1 of compound **6** distributed mainly on the conjugation side chain as shown in Fig. 5E, therefore the transition from HOMO to LUMO+1 can be ascribed to the absorption of the alkynylphenyl chain. However, the absorption of the conjugation side chain in the experimental recorded spectra is at 350 nm, which is obviously shorter in wavelength than the theoretical predication. This might be caused by the disturbance on the conjugation of the side chain because of the solvation during the experiment. The longer the side chain is, the stronger the disturbance will be, and the diversion of the theoretical predication from the experimental results will be more significant just as seen in the calculated results of other compounds in these series.

2.6. Simulated fluorescence spectra

The stable first singlet excited state was obtained by single-excitation configuration interaction CIS/3-21g(d) approach for **1**–**6**. Table 6 lists the structural parameters of the first singlet excited states. From the frequency results, no imaginary frequency appear, so the optimized excited state structures are stable structure on the potential energy surface. Compared the excited state structural parameters with those of the ground states, we can find that the length of the most bonds are reduced little bit in the excited state. Only few examples, such as C_{18}–C_7, C_{12}–C_{17} and C_{10}–C_{11} are increased. The twist angles between two naphthalene rings are decreased in the excited states according to the calculated result.

Table 6
Structure parameter of the first singlet excited state structure of PDI derivatives **1**–**6.**

Parameter	1	2	3	4	5	6
C_1–C_2	1.375	1.376	1.376	1.376	1.376	1.376
C_2–C_3	1.375	1.375	1.374	1.375	1.374	1.374
C_3–C_{13}	1.393	1.392	1.392	1.392	1.392	1.392
C_{18}–C_7	1.437	1.442	1.442	1.442	1.442	1.442
C_7–C_8	1.388	1.398	1.399	1.397	1.399	1.399
C_8–C_9	1.371	1.362	1.361	1.363	1.361	1.361
C_9–C_{20}	1.402	1.411	1.412	1.411	1.412	1.412
C_{20}–C_{19}	1.424	1.424	1.423	1.424	1.423	1.423
C_{20}–C_{10}	1.391	1.384	1.384	1.385	1.384	1.383
C_{10}–C_{11}	1.384	1.386	1.386	1.386	1.386	1.386
C_{11}–C_{12}	1.369	1.368	1.368	1.368	1.368	1.368
C_{12}–C_{17}	1.418	1.415	1.415	1.416	1.415	1.415
C_{17}–C_{15}	1.44	1.445	1.445	1.444	1.445	1.445
C_{19}–C_{17}	1.425	1.424	1.424	1.424	1.424	1.424
C_{19}–C_{18}	1.419	1.418	1.418	1.418	1.418	1.418
C_1–R_1	1.355	1.357	1.357	1.357	1.357	1.357
C_7–R_2	1.424	1.407	1.405	1.408	1.405	1.405
α_1	11.29	11.29	11.26	11.31	11.26	11.26
α_2	15.41	16.62	16.64	16.63	16.64	16.64

Based on the optimized structure of the excited state, we calculated the maximum fluorescence emission wavelength by using TD-b3lyp-6-31g(d) and TD-PBE1PBE-6-31g(d) methods. The calculated results are shown in Table 7. Similar to the calculated absorption spectra, the calculated largest emission wavelengths shifted to longer wavelength with the conjugation chain growth of the substituent, this is in accordance with the experimental results. The calculated results based on TD-b3lyp/6-31g(d) method for **1**, which has short conjugation chain length, show good coincident with the experimental results while the results for the PDIs with longer conjugation chain diverted significantly from the experimental results. Contrarily, the calculated results based on PBE1PBE method for **4** responds to the experimental results well while the calculated results for other compounds in this series present large difference from the experimental results. This results suggest that the calculation on the maximum fluorescence emission by both TD-b3lyp-6-31g(d) and TD-PBE1PBE-6-31g(d) methods do not give satisfied results especially for those with long conjugation side chain. Both methods have over estimated the contribution of the alkynyl or phenyl groups which far away from the PDI core to the whole conjugation system, this has also observed during the absorption spectra simulation.

Fluorescence quantum yield, Φ_f, can be simply expressed as:

$$\Phi_f = \frac{K_f}{K_f + K_{NR}}$$

where K_{NR} is the non-radiative transition rate constant and K_f is the fluorescence radiation rate constant. K_f is closely related with the oscillator strength, f. Large f means quick transition and therefore

Table 7
The calculated largest fluorescence emission wavelength compared with experimental data.

Compound	1	2	3	4	5	6
Expt.	589 nm	604 nm	615 nm	602 nm	612 nm	620 nm
Φ_f (%)	97.2	91	67.6	81	72	76
E/eV	2.11	2.06	2.09	2.06	2.03	2.05
Cal[a]	588 nm	618 nm	663 nm	612 nm	652 nm	680 nm
E[a]/eV	2.109	2.007	1.870	2.027	1.902	1.823
f[a]	0.549	0.469	0.441	0.472	0.436	0.432
Cal[b]	575 nm	612 nm	636 nm	606 nm	637 nm	646 nm
E[b]/eV	2.16	2.03	1.95	2.04	1.95	1.92
f[b]	0.555	0.475	0.477	0.500	0.461	0.481

[a] Calculated by TD-b3lyp/6-31g(d).
[b] Calculated by TD-PBE1PBE/6-31g(d) method.

results in shorter fluorescence lifetime and larger fluorescence quantum yield. The calculated *f* for **1** is 0.55, which is the largest among these PDIs, corresponding well with the experimental recorded largest fluorescence quantum yield and the shortest fluorescence lifetime for **1**. Meaning while, **3** and **5** present the smallest *f* in these series compounds and corresponding well with the smallest experimentally recorded fluorescence quantum yields and longest fluorescence lifetimes of them. It is interesting that both the fluorescence quantum yields and the fluorescence lifetime do not change linearly with the increase of the conjugation length of the substituent.

3. Conclusion

Introduction of alkynylphenyl groups at the bay positions of PDI could vary the photophysical properties of PDI compounds efficiently. The redshifted absorption and emission maximum peaks revealed the participation of the conjugated side chain to the whole conjugation system of the molecule. The quantum calculation on the molecular structure, the orbital energy levels and the frontier orbital maps reveal the electron transfer characteristics for the excited states of these compounds. The simulated absorption and emission spectra for the PDIs with short side conjugation chain shown good coincident with the experimental results. However, along with the increase on the length of the side conjugation chain, the quantum calculation results diverted from the experimental results more and more significantly probably because of the enhanced electron transfer characteristics of the excited states.

4. Experimental

4.1. Materials and methods

N,*N*-dicyclohexyl-1-bromo-7-dodecyl-perylene-3,4,9,10-tetracarboxy diimide (PDI-Br) and *N*,*N*-dicyclohexyl-1,7-bi(4-*tert*-butyl)phenoxy)perylene-3.4,9,10-tetracarboxylic diimide was prepared following the literature methods [27,35], all other chemicals are purchased from commercial source. Solvents were of analytical grades and were purified by the standard method before use.

^{1}H NMR and ^{13}C NMR spectra were recorded on a Bruker DPX 300 spectrometer (300 MHz) in $CDCl_3$. Electronic absorption spectra were recorded on a Hitachi U-4100 spectrophotometer. Fluorescence spectra and the fluorescence life time were measured on a K2 system (ISS product) with the excitation at 410 nm. The fluorescence lifetimes were measured with a phase modulation model with a scattering sample as standard. The fluorescence quantum yields are calculated with *N*,*N*-dicyclohexyl-1,7-bi(4-*tert*-butyl)phenoxy)perylene-3,4,9,10-tetracarboxy diimide as standard. MALDI-TOF mass spectra were taken on a Bruker BIFLEX III ultra-high resolution Fourier transform ion cyclotron resonance (FT-ICR) mass spectrometer. Elemental analyses were performed on a VarioEL III analyzer.

4.1.1. (2-(4-Iodophenyl)ethynyl)trimethysilane (**7**)

A mixture of paradiiodobenzene (0.66 g, 2 mmol), $Pd(PPh_3)_4$ (250 mg, 0.2 mmol), CuI (18 mg, 0.02 mmol), toluene (30 mL) and triethylamine (6 mL) was stirred at room temperature for 5 min under the protection of nitrogen, and then trimethylsilylacetylene (150 μl, 1 mmol) was added to the reaction mixture. The mixture was heated to 50 °C and kept at this temperature for 5 h. Then the solvents were evaporated under reduced pressure. The residue was column chromatographied on silica gel with petroleum ether as eluent. The second fraction was collected. Compound **7** was collected as white solid. Yield: 0.46 g, (38.3%). ^{1}H NMR ($CDCl_3$), (δ: ppm): 7.64 (m, 2H), 7.19 (m, 2H), 0.24 (s, 9H); MALDI-TOF MS (*m*/*z*): Calculated: 300.12; Found: 300. Compound **8** (1,4-bis(2-(trimethysilyl)ethynyl)-benzene was collected from the third fraction. Yield: 0.106 g, (20%). ^{1}H NMR ($CDCl_3$), (δ: ppm): 7.38 (d, 4H), 0.24 (s, 9H).

4.1.2. N,N-dicyclohexyl-1-dodecyl-7-ethynyl-perylene-3,4,9,10-tetracarboxydiimide (**1**)

To a mixture of PDI-Br (81.7 mg, 0.1 mmol), CuI (4 mg, 0.01 mmol), $Pd(PPh_3)_4$ (15 mg, 0.012 mmol), toluene (5 mL), and triethylamine (1 mL) in a 100 ml round bottom flask, trimethylsilylacetylene (30 μL) were added under the protection of nitrogen. The mixture was heated to 50 °C and kept at this temperature for 2 h. The solvents were then evaporated under reduced pressure. The residue was column chromatographied on silica gel with chloroform and *n*-hexane (6:1, v/v) as eluent. The first fraction contains PDI-Si. Yield: 78.7 mg, (94.6%). The PDI-Si was not further purified and characterized but put into next step directly to synthesis compound **1**.

A mixture of PDI-Si (83 mg, 0.1 mol), dried THF (15 mL), and half drop of TBAF was stirred at room temperature for 30 min. The solvents were evaporated under reduced pressure. The residue was column chromatographied on silica gel with chloroform as eluent. **1** was collected as red solid. Yield: 71 mg, (92%). ^{1}H NMR ($CDCl_3$), (δ: ppm): 9.97(d, 1H), 9.45(d, 1H), 8.71 (s, 1H), 8.55 (m, 2H), 8.38 (s, 1H), 5.03 (m, 2H), 4.46 (m, 2H), 3.78 (s, 1H), 2.59 (m, 4H), 2.09–1.26 (m, 36H), 0.87 (t, 3H); ^{13}C NMR (300 MHz $CDCl_3$), (δ: ppm): 163.7, 163.6, 163.3, 163.1, 157.5, 148.0, 137.9, 137.8, 134.8, 134.0, 133.1, 133.1, 131.1, 130.8, 130.1, 128.5, 128.2, 127.8, 127.8, 127.6, 127.5, 124.4, 123.6, 123.3, 122.5, 122.0, 118.3, 117.6, 106.2, 105.0, 70.6, 54.1, 54.0, 31.9, 29.7, 29.6, 29.6, 29.3, 29.2, 29.1, 26.6, 26.3, 25.5, 22.7, 14.1; MALDI-TOF MS (*m*/*z*): Calculated: 763.0; Found: 763.

4.1.3. N,N-dicyclohexyl-1-dodecyloxy-7-(1,4-diethynylbenzene)perylene-3,4,9,10-tetracarboxydiimide (**2**)

A mixture of **1** (38 mg, 0.05 mmol), CuI (2 mg, 5 μL), $Pd(PPh_3)$ (7.5 mg, 6 μL), toluene (5 mL), triethylamine (1 mL) and **7** (24 mg, 0.08 mmol) was heated to 50 °C under the protection of nitrogen. The reaction mixture was kept at this temperature for about 1 h, and then the solvents were evaporated under reduced pressure. The residue was column chromatographied on silica gel with chloroform and *n*-hexane (6:1, v/v) as eluent. The first fraction was collected. The dried compound was dissolved in dried THF (5 mL), and half drop of TBAF. The mixture was stirred at room temperature for 30 min. Then THF was evaporated under reduced pressure. The residue was column chromatographied on silica gel with chloroform as eluent. The first fraction contains **2.** Yield: 25.8 mg, (62%). ^{1}H NMR ($CDCl_3$), (δ: ppm): 9.82 (d, J = 8.1 Hz, 1H), 9.32 (d, 1H), 8.56 (s, 1H), 8.41 (m, 2H), 8.28 (s, 1H), 7.56 (m, 4H), 5.01 (m, 2H), 4.37 (m, 2H), 3.28 (s, 1H), 2.59(m, 4H), 2.05–1.27 (m, 36H), 0.88 (t, 3H); ^{13}C NMR (300 MHz $CDCl_3$), (δ: ppm): 163.6, 163.4, 163.3, 162.9, 157.3, 136.8, 133.5, 132.7, 132.5, 132.3, 131.5, 131.4, 130.7, 130.5, 128.0, 127.9, 127.4, 127.4, 127.0, 126.9, 124.4, 124.2, 123.3, 123.0, 122.6, 122.2, 121.8, 121.5, 119.5, 117.7, 117.2, 97.5, 97.2, 93.0, 83.1, 70.5, 54.2, 54.1, 31.9, 29.7, 29.6, 29.4, 29.4, 29.3, 29.2, 29.1, 26.7, 26.3, 25.6,22.7, 14.1; MALDI-TOF MS (*m*/*z*): Calculated: 863.12; Found: 862.

Compound **2** can also be obtained by following procedures: A mixture of PDI-Br (150 mg, 0.183 mmol), CuI (10 mg, 0.025 mmol), $Pd(PPh_3)$ (25 mg, 0.02 mmol), DMF (50 mL), NaOH (15 mg, 0.375 mmol) and 1,4-dialkynylbenzene (24 mg, 0.183 mmol) was heated to 80 °C under the protection of nitrogen. The reaction mixture was kept at this temperature for about 24 h, and then the solvents were evaporated under reduced pressure. The residue was washed with water thoroughly. The mixture was purified by col-

umn chromatographied on silica gel with chloroform as eluent. Compound **2** (10 mg, 0.012 mmol) was collected from the second fraction with a yield of 6.3%.

4.1.4. N,N-dicyclohexyl-1-dodecyloxy-7-(1,2-bis(4-ethynylphenyl)ethyne)perylene-3,4,9,10-tetracarboxydiimide (**3**)

With **2** (21 mg) as starting material, following the similar procedures of **2**, compound **3** was prepared. Yield: 14.3 mg, (60%). ^{1}H NMR ($CDCl_3$), (δ: ppm): 10.01 (d, J = 8.24 Hz, 1H), 9.505 (d, J = 8.4 Hz, 1H), 8.74 (s, 1H), 8.56 (m, 2H), 8.42 (s, 1H), 7.60 (s, 4H), 7.51 (m, 4H), 5.05 (m, 2H), 4.47 (m, 2H), 3.20 (s, 1H), 2.57 (m, 4H), 2.16–1.26 (36 H), 0.87 (t, 3H); ^{13}C NMR (300 MHz $CDCl_3$), (δ: ppm): 163.5, 163.4, 163.4, 163.1, 132.3, 132.1, 131.9, 131.9, 131.6, 131.5, 128.1, 127.7, 54.2, 54.1, 31.9, 29.7, 29.6, 29.4, 29.3, 29.2, 29.1, 26.6, 26.3, 25.6, 22.7, 14.1; MALDI-TOF MS (m/z): Calculated: 962.8; Found: 962.

4.1.5. N,N-dicyclohexyl-1-dodecyl-7-(4-ethynylbenzene)perylene-3,4,9,10-tetracarboxydiimide (**4**)

A mixture of **1** (38 mg, 0.05 mmol), CuI (2 mg, 5 μL), $Pd(PPh3)_4$ (7.5 mg, 6 μL), iodo-benzene (12.3 mg, 0.06 mmol), toluene (5 mL), and triethylamine (1 mL) was heated to 50 °C at kept at this temperature for about 1 h. Then the solvents were evaporated under reduced pressure. The residue was column chromatographied on silica gel with chloroform as eluent. Compound **4** was collected as red powder. Yield: 12.1 mg, (58%). ^{1}H NMR ($CDCl_3$), (δ: ppm): δ 10.03 (d, J = 8.2 Hz, 1H), 9.46 (d, J = 8.4 Hz, 1H), 8.73 (s, 1H), 8.52 (m, 2H), 8.38 (s, 1H), 7.64 (m, 2H), 7.46 (m, 3H), 5.04 (m, 2H), 4.44 (m, 2H), 2.59 (m, 4H), 2.16–1.26 (m, 36H), 0.85 (t, 3H); ^{13}C NMR (300 MHz $CDCl_3$), (δ: ppm): 163.6, 163.6, 163.5, 163.2, 157.4, 137.0, 133.9, 133.7, 133.1, 131.8, 130.8, 129.4, 128.8, 128.3, 128.2, 127.7, 127.5, 127.3, 127.1, 124.3, 123.3, 123.2, 122.4, 121.9, 121.7, 119.9, 118.4, 117.4, 97.8, 91.3, 54.2, 54.0, 31.9, 29.7, 29.6, 29.4, 29.4, 29.3, 29.2, 29.1, 26.6, 26.3, 25.5, 22.7, 14.1; MALDI-TOF MS (m/z): Calculated: 839.1; Found: 838.

4.1.6. N,N-dicyclohexyl-1-dodecyloxy-7-(1-ethynyl-4-(2-phenylethynyl)benzene)perylene-3,4,9,10-tetracarboxydiimide (**5**)

Following the similar procedure of **4**, with **2** as starting material, compound **5** was prepared. Yield: 12.4 mg, (53%). 1H NMR (CDCl3), (δ: ppm): 9.77 (d, J = 8.2 Hz, 1H), 9.24 (d, 1H), 8.47 (s, 1H), 8.35 (m, 2H), 8.22 (s, 1H), 7.59 (m, 4H), 7.38 (m, 5H), 5.02 (m, 2H), 4.32 (m, 2H), 2.56 (m, 4H), 2.17–1.27 (m, 36H), 0.85 (t, 3H); ^{13}C NMR (300 MHz $CDCl_3$), (δ: ppm): 163.6, 163.5, 163.5, 163.2, 157.4, 136.9, 134.0, 133.7, 133.1, 131.9, 131.8, 131.6, 130.8, 128.6, 128.4, 128.3, 128.2, 127.7, 127.5, 127.4, 127.1, 124.5, 124.3, 123.4, 123.3, 122.9, 122.0, 121.9, 121.7, 119.9, 118.1, 117.4, 97.4, 93.0, 88.9, 86.3, 70.6, 54.2, 54.1, 31.9, 29.7, 29.6, 29.4, 29.4, 29.2, 29.1, 26.6, 26.3, 25.5, 22.7, 14.1; MALDI-TOF MS (m/z): Calculated: 939.2; Found: 938.

4.1.7. N,N-dicyclohexyl-1-dodecyloxy-7-(1-(2-(4-ethynylphenyl)ethynyl)-4-(2-phenylethynyl)benzene)perylene-3,4,9,10-tetracarboxydiimide (**6**)

Following the similar procedure of **4**, with **3** as starting material, compound **6** was prepared. Yield: 8.8 mg, (50%). ^{1}H NMR ($CDCl_3$), (δ: ppm): 9.87 (d, J = 8.2 Hz, 1H), 9.34 (d, 1H), 9.57 (s, 1H), 8.43 (m, 2H), 8.29 (s, 1H), 7.53 (m, 9H), 7.35 (m, 4H), 5.02 (m, 2H), 4.38 (m,2H), 2.60 (m, 4H), 2.16–1.27 (m, 36H), 0.86 (t, 3H); ^{13}C NMR (300 MHz $CDCl_3$), (δ: ppm): 163.4, 163.4, 163.3, 163.0, 157.3, 136.8, 133.7, 133.5, 132.8, 131.9, 131.7, 130.7, 128.5, 128.4, 128.0, 127.9, 127.5, 127.4, 127.1, 126.9, 124.3, 123.6, 123.3, 123.1, 122.7, 122.1, 121.8, 121.5, 119.6, 117.8, 117.2, 97.6, 93.2, 92.0, 91.5, 90.8, 89.1, 77.4, 76.9, 76.6, 70.5, 54.2, 54.1, 31.9, 29.7, 29.7, 29.5, 29.4, 29.3, 29.2, 29.1, 26.7, 26.3, 25.6, 22.7, 14.1; MALDI-TOF MS (m/z): Calculated: 1039.3; Found: 1038.

4.2. Calculation model and method

By Gaussian03 quantum chemical software package [36], we employ b3lyp/6-31g(d) theoretical methods and basis set for these six PDI derivatives structural optimization and vibration analysis. Vibration analysis results show that there is no imaginary frequency appears, so the structures of these PDI derivatives are stable ground state structure. Take advantage of these ground state structure, we use TD-B3lyp/6-31g(d) and TD-PBE1PBE/6-31g(d) to calculate the absorption spectra. Use cis/3-21g(d) optimize the first excited singlet state of these six PDI derivatives. Vibration analysis results show that there is no imaginary frequency appears, so the excited state structure is stable structure. Then we use TD-B3lyp/6-31g(d) and TD-PBE1PBE1/6-31g(d) to calculate the fluorescence emission wavelength. All the calculations were performed using the Gaussian 03 program in the IBM P690 system at the Shandong Province High Performance Computing Centre. With the help of the SWIZARD software [37], the calculated electronic absorption data of **1** and **6**, were simulated to sequential absorption spectrum.

Acknowledgements

Financial support from the Natural Science Foundation of China (Grant Nos. 20640420467, 20771066, 20571049), Ministry of Education of China, Shandong University, is gratefully acknowledged.

References

[1] H.E. Katz, Z. Bao, S.L. Gilat, Acc. Chem. Res. 34 (2001) 359–369.
[2] F. Würthner, Angew. Chem. Int. ED. 40 (2001) 1037–1039.
[3] M.A. Angadi, D. Gosztola, M.R. Wasielewski, Mater. Sci. Eng. B 63 (1999) 191–194.
[4] P. Ranke, I. Bleyl, J. Simmerer, D. Haarer, A. Bacher, H.W. Schmidt, Appl. Phys. Lett. 71 (1997) 1332–1334.
[5] K.Y. Law, Chem. Rev. 93 (1993) 449–486.
[6] B.A. Gregg, R.A. Cormier, J. Am. Chem. Soc. 123 (2001) 7959–7960.
[7] A.J. Breeze, A. Salomon, D.S. Ginley, B.A. Gregg, H. Tillmann, H.H. Horhold, Appl. Phys. Lett. 81 (2002) 3085–3087.
[8] R.T. Hayes, M.R. Wasielewski, D. Gosztola, J. Am. Chem. Soc. 122 (2000) 5563–5567.
[9] W.B. Davis, W.A. Svec, M.A. Ratner, M.R. Wasielewski, Nature 396 (1998) 60–63.
[10] F. Hippiu, F. Schlosser, J. Am. Chem. Soc. 128 (2006) 3870–3871.
[11] K. Tornizaki, R.S.R.S. Loewe, C. Kirmaier, J.K. Schwartz, J.L. Retsek, D.F. Bocian, J. Org. Chem. 67 (2002) 6519–6531.
[12] A. Hagfeldt, M. Gratzel, Acc. Chem. Res. 33 (2000) 269–277.
[13] K. Balakrishman, A. Datar, T. Naddo, J. Huang, R. Oitker, M. Yen, J. Zhao, L. Zhang, J. Am. Chem. Soc. 128 (2006) 7390–7398.
[14] K. Balakrishnan, A. Datar, R. Oitker, H. Chen, J. Zuo, L. Zang, J. Am. Chem. Soc. 127 (2005) 10496–10497.
[15] J. Locklin, D. Li, S.C.B. Mannsfeld, E. Borken, H. Meng, R. Advincula, Z. Bao, Chem. Mater. 17 (2005) 3366–3374.
[16] Z. Chen, M.G. Debije, T. Debaerdemaeker, P. Osswald, F. Würthner, Chemphychem 5 (2004) 137–140.
[17] C.C. Chao, M.K. Leung, Y.O. Su, K.Y. Chiu, T.H. Liu, S.J. Shieh, S.C. Lin, J. Org. Chem. 70 (2005) 4323–4331.
[18] S. Becker, A. Böhm, K. Müllen, J. Chem. Eur. 6 (2000) 3984–3990.
[19] H. Langhals, P. Blanke, Dyes Pigment 59 (2003) 109–116.
[20] M. Sandrai, L. Hadel, R.R. Sauers, S. Husain, K. Krogh-Jespersen, J. Phys. Chem. 96 (1992) 7988–7996.
[21] C. Ego, D. Marsitzkey, S. Becker, J. Zhang, A.C. Grimsdale, J.D. MacKenzie, C. Silva, R.H. Friend, J. Am. Chem. Soc. 125 (2003) 437–443.
[22] W. Qiu, S. Chen, X. Sun, Y. Liu, D. Zhu, Org. Lett. 8 (2006) 867–870.
[23] J.M. Serin, D.W. Brousmiche, J.M.J. Frechet, J. Am. Chem. Soc. 124 (2002) 11848–11849.
[24] J.M. Giaimo, A.V. Gusev, M.R. Wasielewski, J. Am. Chem. Soc. 124 (2002) 8530–8531.
[25] B.A. Jones, M.J. Ahrens, M.H. Yoon, A. Facchetti, T.J. Marks, M.R. Wasielewski, Angew. Chem. Int. Ed. 43 (2004) 6363–6366.
[26] M.J. Ahrens, M.J. Fuller, M.R. Wasilewski, Chem. Mater. 15 (2003) 2684–2686.
[27] C. Zhao, Y. Zhang, R. Li, R. Li, J. Jiang, J. Org. Chem. 72 (2007) 2402–2410.
[28] R. Raramasivan, C. Revital, S. Elijah, J.W. Linda, R. Boris, J. Org. Chem. 72 (2007) 5973–5979.
[29] F. Hadicke, F. Graser, Acta Crystallogr. Sect. C 42 (1986) 189–195.
[30] W. Su, Y. Zhang, C. Zhao, X. Li, J. Jiang, ChemPhysChem 8 (2007) 1857–1862.
[31] A. Dreuw, M. Head-Gordon, Chem. Rev. 105 (2005) 4009–4037.

[32] A. Dreuw, M. Head-Gordon, J. Am. Chem. Soc. 126 (2004) 4007–4016.
[33] Y. Wang, G. Wu, Acta Phys. Chim. Sin. 23 (2007) 1813–1818.
[34] Y. Wang, G. Wu, Acta Phys. Chim. Sin. 24 (2008) 552–560.
[35] M.J. Ahrens, L.E. Sinks, B. Rybtchinski, W. Liu, B.A. Jones, J.M. Giaimo, A.V. Gusev, A.J. Goshe, D.M. Tiede, M.R. Wasielewski, J. Am. Chem. Soc. 126 (2004) 8284–8294.
[36] M.J. Frisch, G.W. Trucks, H.B. Schlegel, G.E. Scuseria, M.A. Robb, J.R. Cheeseman, J. A. Montgomery, Jr., T. Vreven, K.N. Kudin, J.C. Burant, J.M. Millam, S.S. Iyengar, J. Tomasi, V. Barone, B. Mennucci, M. Cossi, G. Scalmani, N. Rega, G.A. Petersson, H. Nakatsuji, M. Hada, M. Ehara, K. Toyota, R. Fukuda, J. Hasegawa, M. Ishida, T. Nakajima, Y. Honda, O. Kitao, H. Nakai, M. Klene, X. Li, J.E. Knox, H.P. Hratchian, J.B. Cross, C. Adamo, J. Jaramillo, R. Gomperts, R.E. Stratmann, O. Yazyev, A.J. Austin, R. Cammi, C. Pomelli, J.W. Ochterski, P.Y. Ayala, K. Morokuma, G.A. Voth, P. Salvador, J.J. Dannenberg, V.G. Zakrzewski, S. Dapprich, A.D. Daniels, M.C. Strain, O. Farkas, D.K. Malick, A.D. Rabuck, K. Raghavachari, J.B. Foresman, J.V. Ortiz, Q. Cui, A.G. Baboul, S. Clifford, J. Cioslowski, B.B. Stefanov, G. Liu, A. Liashenko, P. Piskorz, I. Komaromi, R.L. Martin, D.J. Fox, T. Keith, M.A. Al-Laham, C.Y. Peng, A. Nanayakkara, M. Challacombe, P.M. W. Gill, B. Johnson, W. Chen, M.W. Wong, C. Gonzalez, J.A. Pople, Gaussian 03, Revision B.05, Gaussian, Inc., Pittsburgh, PA, 2003.
[37] S.I. Gorelsky, SWizard program. http://www.sg-chem.net/.